Optical second-harmonic generation selection rules and resonances in buried oxide interfaces: the case of $LaAlO_3/SrTiO_3$

Domenico Paparo,* Andrea Rubano, and Lorenzo Marrucci

CNR-SPIN and Dipartimento di Fisica, Università di Napoli Federico II, Compl. Univ. di Monte S. Angelo, via Cintia, 80126 Napoli, Italy
**Corresponding author: domenico.paparo@spin.cnr.it*

Received April 16, 2013; revised July 23, 2013; accepted July 28, 2013;
posted August 2, 2013 (Doc. ID 188794); published August 23, 2013

Despite an intense research effort, the physical mechanism underlying the formation of a quasi-two-dimensional electron gas at the interface between the band insulators $LaAlO_3$ and $SrTiO_3$ is still not fully understood. Interface-sensitive optical second-harmonic spectroscopy can shed light on this mechanism, by accessing specific information on the orbital and structural reconstruction taking place at the interface that is not accessible by other techniques, and in particular by transport measurements. Here we present a detailed theoretical analysis of the spectral transitions that are most relevant in the second-order nonlinear optical response of oxide interfaces with a square symmetry, in general. In particular, we discuss the case of $LaAlO_3/SrTiO_3$ interfaces, using symmetry arguments to derive specific selection rules, which have strong consequences on the second-harmonic spectra recorded with different input/output polarization combinations of light. These selection rules may in particular explain recent experimental findings.

OCIS codes: (190.0190) Nonlinear optics; (190.4350) Nonlinear optics at surfaces; (240.1485) Buried interfaces; (240.4350) Nonlinear optics at surfaces; (300.6490) Spectroscopy, surface.
http://dx.doi.org/10.1364/JOSAB.30.002452

1. INTRODUCTION

As the semiconductor technology is reaching its natural limit, the miniaturization to the nanoscale strongly challenges the scientific community to find new materials for electronics. To this purpose, oxide heterostructures, such as $LaAlO_3/SrTiO_3$ are promising candidates [1]. Since the discovery that a quasi-two-dimensional electron gas (2DEG) may be formed at the interface between the two band insulators $LaAlO_3$ (LAO) and $SrTiO_3$ (STO) [2], an intense research effort started, which is unveiling a surprising array of unexpected phenomena, ranging from tunable conductivity to two-dimensional superconductivity, and more [3–12]. The 2DEG phenomenon is not limited to this specific interface: other polar oxide heterostructures have shown a similar or related behavior [13–16], thus turning the use of polar-discontinuity effects as a new general strategy for interfacial carrier doping 17]] and nanoscale device manufacturing [18] into a realistic prospect.

However, in spite of intense research efforts, key properties of the 2DEG, like the microscopic mechanisms driving it, are still controversially discussed. A large body of evidence points to the so-called *polar catastrophe scenario* [3] as the mechanism driving the formation of the conducting state. However, many issues remain still open, as, for instance, the prevention of the 2DEG formation when the STO substrate is terminated with a SrO plane. In this case, not considering possible interfacial reconstructions, the SrO-terminated system is structurally identical to the TiO_2-terminated one, except for the two half-unit cells adjacent to the interface on the LAO and STO sides. However, this slight difference is sufficient to have dramatic consequences on the electronic transport properties of the interface. This simple, yet significant example, highlights the need of experimental probes suitable for investigating so-called "buried" interfaces with a nanometer and subnanometer resolution along the interface. So far, only few spectroscopic methods have been applied to the LOA/STO interface, mainly based on electronic or photoelectronic approaches. They have revealed that structural transformations take place in the interfacial region before the onset of conductivity [19,20], but they have not resolved the controversy on whether the charge injection mechanism is dominated by the polar discontinuity or by a simpler "semiconductor-like" band-bending model [9]. The typical probing depth of these spectroscopic techniques is 5–10 nm. A direct standard (linear) optical spectroscopy of the LAO/STO single interface has also been carried out [21], but its interpretation is obviously hindered by the dominance of the bulk signal, since both $LaAlO_3$ and $SrTiO_3$ are wide-gap transparent crystals and their penetration depth at optical frequencies is very large. A more effective way to achieve interface-specific sensitivity approaching a single-monolayer depth is based instead on exploiting the symmetry breaking occurring at the interface, as can be obtained by using second-order nonlinear optics.

Second-order nonlinear optical spectroscopy, such as second-harmonic generation (SHG), is highly interface-specific because it is electric-dipole forbidden in the bulk of centrosymmetric materials [22]. Thus, despite the large penetration depth of light in the material, only the interface (where the symmetry breaking occurs) can contribute significantly to the SHG signal. In other words, SHG provides a

measurement of the degree of polar asymmetry "felt" by all electrons at the interface. In the SHG process, two photons are mixed to create a single photon having double energy. The detected SHG signal, that is the number of emitted double-frequency photons, is proportional to the absolute square of the second-order susceptibility tensor $\hat{\chi}^{(2)}$ characterizing the interface. In the interfacial region between STO and LAO, where the inversion symmetry is broken, some specific $\hat{\chi}^{(2)}$ components are nonzero, as we will show in the following. Recently, the coupling of the SHG signal with the interfacial reorganization taking place in LAO/STO interfaces in connection with the appearance of the 2DEG has been unambiguously demonstrated [23–27]. However many of the specific observations reported in these experiments cannot be explained by merely resorting to the general theory of SHG [28]. Hence the need of developing a specific formalism suitable for LAO/STO interfaces.

A frequent problem in applying the SHG technique is that of establishing a clear interpretative link between the measurable "macroscopic" $\hat{\chi}^{(2)}$ tensor (or its variations) and the microscopic quantities of interest, for example in terms of electronic band occupation and orbital reconstructions. [29,30]. This is certainly the case of the LAO/STO interface and the 2DEG formation. However, this link can be easier to establish when the symmetries of electronic orbitals are used to point out specific selection rules, which apply to certain electronic transitions and not to others. In such cases, the variations of the SHG signal in certain spectral regions can be linked directly to physical changes involving those orbitals possessing the right symmetries. Therefore, in this paper, we report a detailed analysis of the SHG selection rules for the LAO/STO interface symmetry. In particular, we link each single $\hat{\chi}^{(2)}$ element to specific electronic transitions of STO. We find that some of these transitions are only present in one of the $\hat{\chi}^{(2)}$ components. This has important consequences on the SHG spectra recorded at different light-polarization combinations, as observed in a very recent experiment [27]. We show that the experimental findings of the latter work can be explained by exploiting the analysis reported here.

We stress that much of our analysis is not limited to the case of LAO/STO interfaces, but it may be readily applied to a wider range of polar/nonpolar interfaces that share the same symmetry properties.

2. SHG THEORY FOR INTERFACES WITH 4 mm (SQUARE) SYMMETRY

SHG is the nonlinear process giving rise to a light wave with doubled frequency 2ω from an incident wave of frequency ω. The constitutive equation of the process, representing the material response, is

$$P_i(2\omega) = \varepsilon_0 \chi_{ijk}(2\omega) E_j(\omega) E_k(\omega), \tag{1}$$

where $\mathbf{P}(2\omega)$ is the induced nonlinear optical polarization, $\mathbf{E}(\omega)$ is the local (complex) electric field of the incident wave in the interface, and the tensor $\hat{\chi}$ is the SHG susceptibility (here and in the following we omit the superscript (2) for brevity). We assume here and in the following that the tensor $\hat{\chi}$ is nonzero only within a thin interfacial (polar) region in which the inversion symmetry is removed, while both the substrate (the STO) and the deposited thin film (the LAO) are centrosymmetric and hence have a vanishing $\hat{\chi}$. Moreover, in the wake of previous results [25], we neglect the possible contribution to SHG of the free (LAO) surface, which in principle could also be polar.

The electronic properties of the polar interface are reflected in the spectral behavior of the nonzero tensor components of $\hat{\chi}$. The actual measured quantity in SHG spectroscopy is the SHG intensity I_{SHG} as a function of the incident photon energy ω, which is proportional to the square of the reflected SHG electric field: $I_{\mathrm{SHG}} \propto |E_{\mathrm{SHG}}|^2$. Exploiting Eq. (1) and the theory of light propagation through stratified media, the latter can, in turn, be written as a function of the incident electric field:

$$E_{\mathrm{SHG}} = \frac{i\omega E_0^2}{\epsilon_0 c \cos\beta} \chi_{\mathrm{eff}}, \tag{2}$$

where c is the speed of light in vacuum, ϵ_0 is the dielectric constant in vacuum, E_0 is the electric field amplitude of the impinging wave, β is the incidence angle, and χ_{eff} is defined as follows:

$$\chi_{\mathrm{eff}} = \int e_i^{\mathrm{out}} L_{ii}^{\mathrm{out}} \chi_{ijk} L_{jj}^{\mathrm{in}} L_{kk}^{\mathrm{in}} e_j^{\mathrm{in}} e_k^{\mathrm{in}} \mathrm{d}z, \tag{3}$$

$\mathbf{e}^{\mathrm{in,out}}$ being the optical polarization unit vectors in vacuum (or in air, if the small refractive index difference is neglected) of the input and output waves, respectively, and $\mathbf{L}^{\mathrm{in,out}}$ are the corresponding Fresnel transformation matrices accounting for the propagation from/to the outside of the medium to/from the polar interface. Here the sum over repeated indices is understood and the z integral is extended across the entire thickness of the polar interface, assumed to be much thinner than the optical wavelength λ. In other words, χ_{eff} defines a suitable combination of $\hat{\chi}$ tensor components inside the material defined by the input/output light polarizations and accounting for all transmission/reflection effects through the boundaries.

A. SHG Angular Dependence

Let us now introduce a Cartesian reference system with the z axis perpendicular to the interface, and x and y in the interface plane, oriented so that xz is the light incidence plane. We assume that both input and output waves are linearly polarized, with an arbitrary polarization angle α (not necessarily the same) with respect to the incidence plane (xz). The electric field unit vectors are then the following:

$$\begin{aligned} \mathbf{e}^{\mathrm{in}} &= (\cos\alpha\cos\beta, \sin\alpha, \cos\alpha\sin\beta), \\ \mathbf{e}^{\mathrm{out}} &= (-\cos\alpha\cos\beta, \sin\alpha, \cos\alpha\sin\beta). \end{aligned} \tag{4}$$

We introduce also the following short notations for specific polarizations: p for a field parallel to the incidence plane ($\alpha = 0$), s for a field parallel to the interface plane ($\alpha = \pi/2$), and d for a field oriented at 45° between p and s ($\alpha = \pi/4$).

Neglecting the reflection effects of the thin LAO layer, the three nonzero components of the diagonal tensor $\mathbf{L}$ can be approximated by the following expressions:

$$L_{xx} = \frac{2\cos\beta'}{n\cos\beta + \cos\beta'},$$
$$L_{yy} = \frac{2\cos\beta}{\cos\beta + n\cos\beta'},$$
$$L_{zz} = \frac{2\cos\beta}{n(n\cos\beta + \cos\beta')}, \tag{5}$$

where n is the refractive index of the SHG-active interface and of the substrate, here assumed to be equal (this corresponds to locating the SHG active region inside the STO substrate, or alternatively to neglecting the refractive index difference between LAO and STO), and β' the propagation (refraction) angle inside the medium. Let us also note that these quantities depend on the frequency, so they in general have different values for the fundamental and second-harmonic light.

B. Tensor Components

Since the crystal structure of the material is perovskite-like, a LAO/STO interface has a fourfold square rotation symmetry and mirror planes along the two principal symmetry axes. Therefore it belongs to the 4 mm Laue group (in Hermann–Mauguin notation, or C_{4v} in Schoenflies notation). Within the 4 mm symmetry, it is easy to show that only the following three independent nonvanishing tensor components are allowed for the $\hat{\chi}$ tensor:

$$\chi_{zzz}$$
$$\chi_{zxx} = \chi_{zyy}$$
$$\chi_{xxz} = \chi_{yyz} = \chi_{xzx} = \chi_{yzy}.$$

From Eqs. (3) and (4) it is easy to see that the last two components can be singled out in χ_{eff} by an appropriate choice of the input and output polarizations, while the diagonal component χ_{zzz} is always present in combination with the other two. In particular, we report the expression of χ_{eff} for the s-input p-output (sp) and the d-input s-output (ds) polarization combinations, which contain χ_{zxx} and χ_{xxz}, respectively, and for the p-input p-output (pp) combination, which contains all three components:

$$\chi^{\text{eff}}_{sp} = \chi_{zxx} t L^{\text{out}}_{zz} (L^{\text{in}}_{yy})^2 \sin\beta,$$
$$\chi^{\text{eff}}_{ds} = \chi_{xxz} t L^{\text{out}}_{yy} L^{\text{in}}_{yy} L^{\text{in}}_{zz} \sin\beta,$$
$$\chi^{\text{eff}}_{pp} = \chi_{zzz} t L^{\text{out}}_{zz} (L^{\text{in}}_{zz})^2 \sin^3\beta + (\chi_{zxx} d L^{\text{out}}_{zz} L^{\text{in}}_{xx} - 2\chi_{xxz} t L^{\text{out}}_{xx} L^{\text{in}}_{zz}) L^{\text{in}}_{xx} \sin\beta\cos^2\beta, \tag{6}$$

in which t denotes the effective thickness of the polar interface and the χ_{ijk} in this expression are actually space-averaged quantities across this thickness.

Using the approximate value of 2.3 for the STO refractive index at the fundamental wavelength (around 800 nm) and of 2.4 for the SHG (at around 400 nm), one can calculate that the coefficient in front of the χ_{zzz} component in the χ^{eff}_{pp} expression is about a factor 20 smaller than the coefficients in front of χ_{xxz} and χ_{xzx} for $\beta = 45°$; for $\beta = 80°$ (about grazing incidence), this coefficient ratio is still about 10. This implies that it is not possible to isolate experimentally the χ_{zzz} contribution, which can only be estimated *a posteriori* once χ_{xxz} and χ_{zxx} are determined, by a delicate subtraction procedure. This has been done for example in [25]. Finally, we stress that any deviation of the interface from the cubic symmetry due, for example, to an interfacial structural reorganization might result in the appearance of other tensor components that complicate our analysis. Although interesting for applications, this case will not be further discussed in the following.

3. RESONANT STRUCTURE OF χ

The general expression for the $\hat{\chi}$ tensor components, in case of a single-electron system within the electric-dipole approximation is the following [31]:

$$\chi^{(2)}_{ijk}(2\omega,\omega,\omega) = \frac{N}{2\hbar^2}\sum_{lmn}\rho^0_{ll}\Bigg[\frac{\mu^i_{ln}(\mu^j_{nm}\mu^k_{ml} + \mu^k_{nm}\mu^j_{ml})}{(\omega_{nl} - 2\omega - i\gamma_{nl})(\omega_{ml} - \omega - i\gamma_{ml})} + \frac{\mu^i_{nm}(\mu^j_{ln}\mu^k_{ml} + \mu^k_{ln}\mu^j_{ml})}{(\omega_{mn} - 2\omega - i\gamma_{mn})(\omega_{nl} + \omega + i\gamma_{nl})} + \frac{\mu^i_{nm}(\mu^j_{ln}\mu^k_{ml} + \mu^k_{ln}\mu^j_{ml})}{(\omega_{nm} + 2\omega + i\gamma_{nm})(\omega_{ml} - \omega - i\gamma_{ml})} + \frac{\mu^i_{ml}(\mu^j_{ln}\mu^k_{nm} + \mu^k_{ln}\mu^j_{nm})}{(\omega_{ml} + 2\omega + i\gamma_{ml})(\omega_{nl} + \omega + i\gamma_{nl})}\Bigg], \tag{7}$$

where N is the number-density of single-electron systems, l, m, n label three arbitrary electronic states, $\omega_{nm} = (E_n - E_m)/\hbar$ is the Bohr frequency associated with the $n \to m$ transition, $\gamma_{nm} = \gamma_{mn}$ is the corresponding dissipation factor determining the linewidth, $\mu^i_{nm} = \langle\psi_n|(-e)x_i|\psi_m\rangle$ is the i–Cartesian component of the transition dipole moment, and ρ^0_{nn} is the diagonal density matrix element denoting the equilibrium population in state n. Assuming that only the ground state g is occupied at equilibrium (low temperature limit), we can slightly simplify the expression above by replacing l with g and removing the sum on l and the population term.

For a multielectron system, Eq. (7) is still valid, but the energy levels now refer to the entire multielectron system, the dipole moments are summed over all electrons and we must set $N = 1/V$, with V being the system volume. Each full-system dipole moment can then be rewritten in terms of single-electron dipole moments as follows:

$$\mu^i_{nm} = \sum_{\text{allel},j}\langle\psi_n|(-e)x_{j,i}|\psi_m\rangle = \sum_{pq}\langle p|(-e)x_{1,i}|q\rangle\langle\psi_n|\hat{a}^\dagger_p\hat{a}_q|\psi_m\rangle = \sum_{pq}\mu^i_{pq}\delta_{\psi_n,\psi_{m-q+p}}, \tag{8}$$

where pq are single-electron states, $\mu^i_{pq} = \langle p|(-e)x_{1,i}|q\rangle$ is now the single-electron transition dipole moment, and the final delta-terms are nonvanishing only if the multielectron state ψ_m becomes equal to ψ_n after subtracting an electron in the state q and adding it in the state p. Therefore, each dipole moment reintroduces a sum over initial and final single-electron states, while the delta term removes the sum over the final multielectron states (as for each pair pq and given initial multielectron state, there is only one possible final multielectron state obtained by removing an electron in q and placing it in p). However, it is necessary to consider the role of the Pauli exclusion principle in the dipole moment sum. This means that, at each transition, the initial single-electron state must be occupied and the final one empty, unless the two states coincide. Having this in mind, the different classes of

contributing transitions can be represented as in Fig. 1, using a form of Feynman's diagrams.

Let us discuss the contribution of each of these diagrams to the $\hat{\chi}$. For a quantitative evaluation, all the following expressions should be turned into multiple integrals over the electron crystal momentum across the Brillouin zone (BZ), but in the present work we are interested only in a qualitative analysis of the resonances and selection rules, so for simplicity we will keep the discrete sum form.

The diagram (A) can be interpreted as a process in which an electron-hole pair in states p and q, respectively, is first created by absorbing a photon, the electron is then promoted to another state r by absorbing another photon and finally recombines with the hole by emitting the SHG photon. All these transitions must be considered as "virtual," as they do not have to conserve energy (as normal, in nonrelativistic perturbation theory). The diagram corresponds to the following $\hat{\chi}$-term:

$$\chi^{A}_{ijk}(2\omega,\omega,\omega) = \frac{1}{2V\hbar^2}\sum_{qpr}\Big\{f(E_q)[1-f(E_p)][1-f(E_r)] \times\Big[\frac{\mu^i_{qr}(\mu^j_{rp}\mu^k_{pq}+\mu^k_{rp}\mu^j_{pq})}{(\omega_{rq}-2\omega-i\gamma_{rq})(\omega_{pq}-\omega-i\gamma_{pq})} + \frac{\mu^i_{rp}(\mu^j_{qr}\mu^k_{pq}+\mu^k_{qr}\mu^j_{pq})}{(\omega_{pr}-2\omega-i\gamma_{pr})(\omega_{rq}+\omega+i\gamma_{rq})} + \frac{\mu^i_{rp}(\mu^j_{qr}\mu^k_{pq}+\mu^k_{qr}\mu^j_{pq})}{(\omega_{rp}+2\omega+i\gamma_{rp})(\omega_{pq}-\omega-i\gamma_{pq})} + \frac{\mu^i_{pq}(\mu^j_{qr}\mu^k_{rp}+\mu^k_{qr}\mu^j_{rp})}{(\omega_{pq}+2\omega+i\gamma_{pq})(\omega_{rq}+\omega+i\gamma_{rq})}\Big]\Big\}, \quad (9)$$

where $f(E)$ is the zero-temperature Fermi distribution, i.e., $f(E)=1$ for $E<E_f$ and $f(E)=0$ otherwise. The diagram (B) represents a similar electronic process, with the difference that the intermediate step involves the hole changing state, rather then the electron. It corresponds to the following $\hat{\chi}$-term:

$$\chi^{B}_{ijk}(2\omega,\omega,\omega) = \frac{1}{2V\hbar^2}\sum_{qpr}\Big\{f(E_q)f(E_r)[1-f(E_p)] \times\Big[\frac{\mu^i_{rp}(\mu^j_{qr}\mu^k_{pq}+\mu^k_{qr}\mu^j_{pq})}{(\omega_{pr}-2\omega-i\gamma_{pr})(\omega_{pq}-\omega-i\gamma_{pq})} + \frac{\mu^i_{qr}(\mu^j_{rp}\mu^k_{pq}+\mu^k_{rp}\mu^j_{pq})}{(\omega_{rq}-2\omega-i\gamma_{rq})(\omega_{pr}+\omega+i\gamma_{pr})} + \frac{\mu^i_{qr}(\mu^j_{rp}\mu^k_{pq}+\mu^k_{rp}\mu^j_{pq})}{(\omega_{qr}+2\omega+i\gamma_{qr})(\omega_{pq}-\omega-i\gamma_{pq})} + \frac{\mu^i_{pq}(\mu^j_{rp}\mu^k_{qr}+\mu^k_{rp}\mu^j_{qr})}{(\omega_{pq}+2\omega+i\gamma_{pq})(\omega_{pr}+\omega+i\gamma_{pr})}\Big]\Big\}. \quad (10)$$

The other diagrams are disconnected (certainly nonresonant) processes, in which two or more of the electronic states involved in the transition coincide. These cases are represented as closed loops and describe the interaction of the photon with static polarization. In particular, diagrams (C) and (D) together correspond to the following $\hat{\chi}$-term:

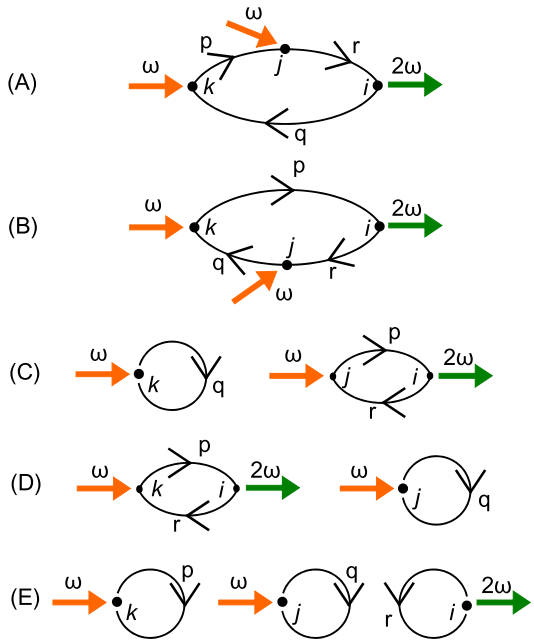

Fig. 1. Feynman's diagrams showing all possible electronic transition paths for SHG. The solid-line arrows going from left to right stand for an initially empty electron state, those going from right to left stand for an initially empty hole state (i.e., occupied electron state), the dots (graph vertices indicated with italic letters) stand for the transition dipoles with the specified Cartesian index. (A) and (B) refer to the nondegenerate cases, occurring when all three states are different, and the eight possible permutations of the vertices correspond to the eight terms appearing in Eq. (7). (C)–(E) correspond to the degenerate cases in which two or all three states coincide.

$$\chi^{CD}_{ijk}(2\omega,\omega,\omega) = \frac{1}{2\hbar^2}\sum_{pr}\Big\{f(E_r)[1-f(E_p)] \times\Big[\mu^i_{pr}(\mu^j_{rp}P^k+\mu^k_{rp}P^j) \times\Big(\frac{1}{(\omega_{rp}-2\omega-i\gamma_{rp})(\omega_{pr}+\omega+i\gamma_{pr})} + \frac{1}{(\omega_{rp}+2\omega+i\gamma_{rp})(\omega_{pr}-\omega-i\gamma_{pr})}\Big) + \frac{P^0_i(\mu^j_{rp}\mu^k_{pr}+\mu^k_{rp}\mu^j_{pr})}{2\omega} \times\Big(\frac{1}{\omega_{pr}+\omega+i\gamma_{pr}}+\frac{1}{\omega_{pr}-\omega-i\gamma_{pr}}\Big)\Big]\Big\}, \quad (11)$$

where $\mathbf{P}^0$ is the static polarization, whose components $P^0_k = (1/V)\sum_q f(E_q)\mu^k_{qq}$ are nonvanishing only for $k=z$. Finally, the χ-term associated with the fully disconnected diagram (E) vanishes identically. We notice that our diagrams are nonstandard for nonlinear optics (while they are more similar to relativistic field-theory diagrams), because they highlight the occupation state of involved electron orbitals, thus explicitly distinguishing between electron and hole transitions. Moreover, many past theoretical treatments of the nonlinear optical susceptibility consider only terms involving two empty intermediate states (electrons) and one filled one (hole), as in our A diagram. The need for including also the contribution of

transitions involving two occupied states (two holes) and an empty one (electron), corresponding to our diagram B, was for example discussed in [32]. However, our treatment is even more general in the fact that it includes also the possible contribution of diagonal dipole-moment matrix elements (allowed in noncentrosymmetric media), which are those giving rise to the disconnected diagrams C and D, and includes dissipative factors in the energy denominators.

4. RESONANCES AND SYMMETRIES

Let us now discuss the possible resonances of the $\hat{\chi}$ tensor, exploiting the 4 mm symmetry of the LAO/STO interfaces. As mentioned, we assume that the bulk system is perfectly centrosymmetric, while the inversion symmetry is broken at the interface, only along the z direction normal to the interface. We also assume that the effect of this symmetry lowering on the electronic states cannot be very large, and thus only one inversion-symmetry-breaking dipole moment is allowed. These assumptions imply that the interfacial electronic states are still either even or odd with respect to the x, y directions (two σ_v inversion planes), while the parity with respect to the z direction is broken. It is also important to underline that the full 4 mm symmetry holds only at the Γ point of the BZ (in which the crystal momentum $\mathbf{k} = 0$), while elsewhere the symmetry is partly broken by the crystal momentum $\mathbf{k}$.

The 4 mm group has five different irreducible representations, named A_1, A_2, B_1, B_2, and E [33]. The first four are singlet states and the last one is a doublet. A_1 is the fully symmetric state, which behaves as 1, z or z^2; A_2 is odd with respect to both σ_v and σ_d inversion planes, and behaves as the rotation matrix R_z; B_1 is odd with respect to $\pi/2$ rotations and σ_d inversions, and behaves as $x^2 - y^2$; B_2 is odd with respect to $\pi/2$ rotations and σ_v inversions, and behaves as xy; finally, the doublet E behaves as the variables x, y or the products xz, yz.

Let us now define two resonant single-electron states a and b, n being any nonresonant state, and assume that $E_a < E_b$ so to have $\omega_{ab} > 0$. The resonance can in principle involve either the fundamental frequency ω or the second-harmonic 2ω.

Let us consider first a ω resonance. We have then $\omega \simeq \omega_{ab}$. By keeping only the resonant terms, the total $\hat{\chi}$ expressions (adding up all terms) can be then simplified as follows:

$$\chi_{ijk}(2\omega,\omega,\omega) = \frac{f(E_a)[1-f(E_b)]}{2\hbar^2(\omega_{ba}-\omega-i\gamma_{ba})} \times \left\{ \frac{1}{V} \sum_{na\neq n\neq b} \left[(1-2f(E_n)) \times \left(\frac{\mu^i_{an}(\mu^j_{nb}\mu^k_{ba}+\mu^k_{nb}\mu^j_{ba})}{\omega_{na}-2\omega-i\gamma_{na}} + \frac{\mu^i_{nb}(\mu^j_{an}\mu^k_{ba}+\mu^k_{an}\mu^j_{ba})}{\omega_{nb}+2\omega+i\gamma_{nb}} \right) \right] + \frac{P^0_i(\mu^j_{ab}\mu^k_{ba}+\mu^k_{ab}\mu^j_{ba})}{-2\omega} + \frac{\mu^i_{ab}(P^0_j\mu^k_{ba}+P^0_k\mu^j_{ba})}{\omega_{ab}+2\omega+i\gamma_{ab}} \right\}. \quad (12)$$

Note that the first sum over n involves both full and empty states, with an opposite sign. This implies that a must be an initially full state (energy below the Fermi level) and b an initially empty state (energy above the Fermi level). Moreover, we may use the standard symmetry representation theory to obtain the selection rules which apply to the transition dipole moment $\int \mu^i_{ab}$ [33]. Putting all together, for a ω resonance among states a and b, we have the following constraints:

$$\begin{aligned} &a, \text{must be an initially full state;} \\ &b, \text{must be an initially empty state;} \\ &\chi_{zzz} \neq 0, \chi_{zxx} = 0, \chi_{xxz} \neq 0, \quad \text{if } a, b \text{ have the same symmetry;} \\ &\chi_{zzz} = 0, \chi_{zxx} \neq 0, \chi_{xxz} \neq 0, \quad \text{if } a, b \text{ have different symmetry,} \\ &\qquad\qquad \text{one being } E; \\ &\chi_{zzz} = 0, \chi_{zxx} = 0, \chi_{xxz} = 0, \quad \text{if } a, b \text{ have different symmetry,} \\ &\qquad\qquad \text{not } E. \end{aligned} \quad (13)$$

It is interesting to check also which additional nonresonant states n may contribute to the sum appearing in Eq. (12). If a, b have the same symmetry, then the states n contributing to χ_{zzz} are all states having also the same symmetry as the resonant ones, while the states n contributing to χ_{xxz} have different symmetry from the resonant ones (in addition, n must be E if a and b are not E). If a, b have different symmetry, one being E, then all states n must have the same symmetry of a or of b to contribute to both χ_{xxz} and χ_{zxx}. The above discussed selection rules are summarized in Table 1.

Let us now analyze the 2ω resonance case. The simplified expression that we find is the following:

Table 1. List of the Selection Rules that Apply for Each χ Element and for Each Kind of Transition (Fundamental or Second-Harmonic Frequency)[a]

χ^2 Elements	Resonant State a	Resonant State b	Nonresonant State n
	ω resonance		
χ_{zzz}	S	S	S
	E	E	E
χ_{zxx}	S	E	E
	S	E	S
	E	S	E
	E	S	S
χ_{xxz}	S	S	E
	E	E	S
	S	E	S
	S	E	E
	E	S	S
	E	S	E
	2ω resonance		
χ_{zzz}	S	S	S
	E	E	E
χ_{zxx}	S	S	E
	E	E	S
χ_{xxz}	S	E	S
	E	S	S
	E	S	E
	S	E	E

[a]In the table, the symbol S refers to any possible singlet symmetry (A_1, A_2, B_1, B_2), but once selected a given symmetry, it must be the same in the entire row.

$$\chi_{ijk}(2\omega,\omega,\omega) = \frac{\mu^i_{ab}}{2V\hbar^2(\omega_{ba}-2\omega-i\gamma_{ba})} \cdot \Bigg\{ f(E_a)[1-f(E_b)]\sum_n \Bigg[\frac{1-f(E_n)}{\omega_{na}-\omega-i\gamma_{na}} + \frac{f(E_n)}{\omega_{bn}-\omega-i\gamma_{bn}} \Bigg] (\mu^j_{bn}\mu^k_{na}+\mu^k_{bn}\mu^j_{na}) + [1-f(E_a)][1-f(E_b)]\sum_n f(E_n)(\mu^j_{na}\mu^k_{bn} + \mu^k_{na}\mu^j_{bn}) \Bigg(\frac{1}{\omega_{an}+\omega+i\gamma_{an}} - \frac{1}{\omega_{bn}-\omega-i\gamma_{bn}} \Bigg) + f(E_a)f(E_b)\sum_n [1-f(E_n)](\mu^j_{na}\mu^k_{bn} + \mu^k_{na}\mu^j_{bn}) \Bigg(\frac{1}{\omega_{an}+\omega+i\gamma_{an}} - \frac{1}{\omega_{bn}-\omega-i\gamma_{bn}} \Bigg) \Bigg\} - \frac{\mu^i_{ba}}{2\hbar^2(\omega_{ba}-2\omega-i\gamma_{ba})} f(E_a)[1-f(E_b)] \frac{\mu^j_{ab}P^0_k + \mu^k_{ab}P^0_j}{\omega_{ba}-\omega-i\gamma_{ba}}. \quad (14)$$

Here, the first term in curly brackets contributes only if a is an occupied state and b an empty one, and so does the last term in the full expression. The second (third) term in curly brackets contributes only if both are empty (filled) states. In order to single out the nonzero components of the $\hat{\chi}$ tensor, we should look at Eq. (14) with the following rules in mind: the dipole moments involving the z coordinate are nonzero only if the two involved states have the same symmetry, since z does not change any parity, and the dipole moments involving x (y) coordinate can be nonzero only between a singlet state of A_1, A_2, B_1, or B_2 symmetry and a doublet state having E symmetry. Therefore we have the following outcome:

$$\begin{aligned} &\chi_{zzz}\neq 0, \chi_{zxx}\neq 0, \chi_{xxz}=0, && \text{if } a,b \text{ have the same symmetry} \\ &\chi_{zzz}=0, \chi_{zxx}=0, \chi_{xxz}\neq 0, && \text{if } a,b \text{ have different symmetry, one being } E \\ &\chi_{zzz}=0, \chi_{zxx}=0, \chi_{xxz}=0, && \text{if } a,b \text{ have different symmetry, not } E. \end{aligned} \quad (15)$$

Also in this case, we can check which conditions the nonresonant states n must satisfy in order to contribute to the sum appearing in Eq. (14). If a, b have the same symmetry, then the n-states contributing to χ_{zzz} must do the same, while the n-states which are contributing to χ_{zxx} must have a different symmetry from the one of a, b, and in addition n must have E symmetry if a, b have another one. If a and b have a different symmetry, one being E, then the n-states contributing to χ_{xxz} must have the symmetry of either a or b. In addition, the n-states can be both filled or empty if a is filled and b is empty. If both are empty then the n-states must be filled, if both are filled, then the n-states must be empty. For this reason, the contribution of these empty–empty and filled–filled transitions are probably minor, since they typically involve larger Bohr-frequency denominators. The above discussed selection rules are summarized in Table 1.

A. Optical Transitions at the Γ-Point of LAO/STO Interfaces

Let us now exploit the rules summarized in Table 1 to link each $\hat{\chi}$ element to a specific atomic orbital character of the real bands at the LAO/STO interface. According to [27], in the range of energy of the SHG photon up to 4.2 eV, the main source of the observed SHG signal resides in the STO side of the interface (note that, coherently with the aforementioned works, our energy scale refers to two-photon energy). This is due to the vicinity of the investigated spectral range to the optical-gap energy of bulk STO. Therefore, in this energy range the SHG signal mainly resides in electronic states close to the valence-to-conduction band edge of STO. The optical-gap energy of LAO is around 5.5 eV and hence the spectral signatures of LAO are expected to manifest themselves in an interval of SHG photon energies corresponding to UV wavelengths. However, this range is hardly accessible with standard SHG experiments because of air absorption and lack of polarization optical components suitable for the UV range. Therefore we will limit our discussion to the spectral features that can be observed by means of standard SHG setups, such as the optical transitions occurring in STO. Nevertheless, we stress that the symmetry-based results presented in the previous section are more general and the following discussion may be easily extended to other material systems having a similar symmetry and crystal structure.

We recall that, under electric dipole approximation, no SHG contribution can arise from the STO centrosymmetric bulk, so we will start describing the bulk band structure and subsequently the changes that are expected because of the interface-induced symmetry breaking. The bulk STO optical gap is known to be associated mainly with a transition from the oxygen $2p$ orbitals to the titanium $3d$-t_{2g} ones. The STO electronic band structure has been calculated, for example, in [34–36].

At the Γ point of the bulk BZ, these bands may be grouped in three levels depending on the relative arrangement of the $2p$ orbitals, as schematically shown in Fig. 2: bonding, nonbonding, and antibonding. Each of these levels is threefold degenerate in the bulk, owing to the cubic symmetry of the crystal. The minimum optical (vertical) transition energy, at the Γ point, is known to be 3.75 eV. The one at the X point is only slightly higher, about 1 eV, and has a similarly high joint density of states. Therefore, it might contribute with additional visible features in the SHG spectra.

The conduction band is predominantly composed of Ti $3d$-t_{2g} orbitals. Because of the cubic crystal field produced by the six nearest-neighbor O atoms, the empty Ti $3d$ orbitals will split into three lower energy t_{2g} orbitals (xy, yz, zx) and two much higher energy e_g orbitals ($3z^2-r^2$, x^2-y^2) [37]. The t_{2g}-e_g splitting of the Ti $3d$ orbitals is of about 2 eV. The strontium $4d$ bands have their peak density of states about 5 eV above the Ti bands. The symmetry lowering from a cubic 3D symmetry to the square 2D one (4 mm) further splits the Γ point bands. In particular, the three Ti $3d$-t_{2g} orbitals (corresponding to d_{xy}, d_{xz}, d_{yz}) should split into two different levels: the orbital d_{xy} with symmetry B_2 and the two degenerate orbitals d_{xz} and d_{yz} forming together an E doublet. The two Ti $3d$-e_g orbitals, in turn, split into an A_1 and B_1 singlets, namely d_{z^2} and $d_{x^2-y^2}$. On the other hand, the three oxygen levels are split into six distinct levels, three singlets and three

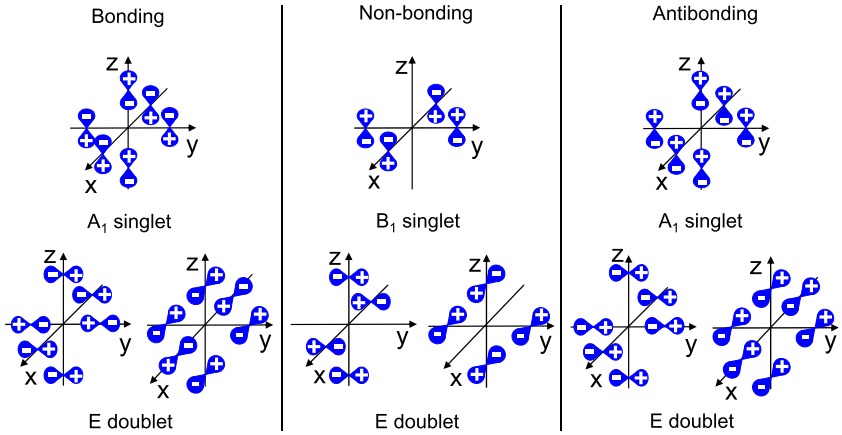

Fig. 2. Possible arrangements of O (2*p*) orbitals forming the nine uppermost valence bands are indicated. Note that in the bulk, at the Γ point in the BZ, these orbitals are grouped in three threefold-degenerate levels (here separated by vertical lines) according to the cubic symmetry. At surface this degeneracy is partly lifted with the separation among singlet and doublet states. It should be also noted that orbitals sharing the same symmetry character (e.g., bonding and antibonding orbitals) can be partly hybridized in the actual energy–eigenvalue states and the exact weight of their contributions cannot be determined by symmetry and can only be computed by numerical methods.

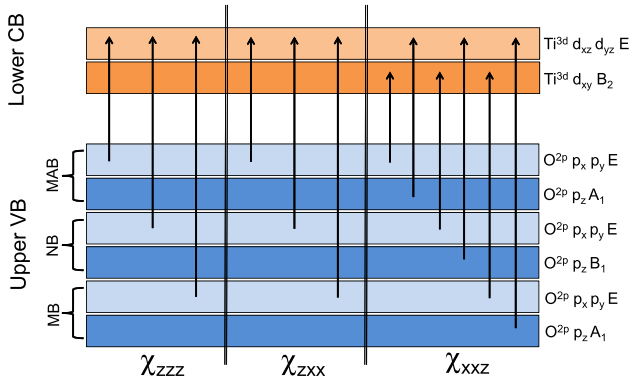

Fig. 3. Symmetry-allowed O(2*p*)-Ti(3*d*) 2ω transitions for all three symmetry-allowed χ_{ijk} components within the 4 mm symmetry group are shown. Note that the allowed transitions for χ_{zzz} (contributing to the *pp* signal together with the other $\hat{\chi}$ elements) and χ_{zxx} (*sp* signal) are the same, whereas two different transitions are allowed for χ_{xxz} (*ds* signal).

doublets. Considering the center of the cubic cell to be placed on the Ti ion, the orbitals of the oxygens lying along the *z* direction (vertical axis of the octahedron) give rise to an A_1 singlet band (p_z) and a E doublet band (p_x, p_y), while the orbitals of the oxygens lying in the TiO_2 plan can be combined into an A_1 band, made of parallel p_z orbitals, a B_1 band, made of antiparallel p_z orbitals, and two different E doublets formed by the p_x and p_y orbitals (see Fig. 2).

We can now add to Table 1 the indication of the most likely electronic transitions contributing to each $\hat{\chi}$ element at the Γ-point. The results are summarized in Fig. 3 and Table 2, where the optical transitions expected to be lowest energy are further highlighted with a diamond symbol (◇). We note that this table does not include possible O–O and Ti–Ti resonant transitions involving empty–empty or filled–filled states. However, we cannot completely exclude that such transitions give some additional, probably minor, contribution to the SHG spectra.

5. DISCUSSION

From the previous analysis of band symmetries and selection rules, we can deduce some qualitative results on the SHG polarization behavior for the various transitions. For example, we see that χ_{zzz} and χ_{zxx} must have exactly the same 2ω resonances, while the χ_{xxz} has different ones. Therefore, the *sp* and *ds* polarization combinations, in particular, should give rise to fairly different spectra (while the *pp* combination is

Table 2. List of all the Nonvanishing Tensor Components (Left Column) Associated to the Most Likely 2ω-Transitions between Resonant States *a* and *b*, Through Nonresonant State *n* (Rows) at the Γ Point of the BZ[a]

χ^2 Elements	Resonant State a	Resonant State b	Nonresonant State n	
χ_{zzz}	O p_z (A_1)	Ti-e_g d_{z^2} (A_1)	A_1	
	O p_z (B_1)	Ti-e_g $d_{x^2-y^2}$ (B_1)	B_1	
	O p_x, p_y (3 E dup.)	Ti-t_{2g} d_{xz}, d_{yz} (E)	E	◇
χ_{zxx}	O p_z (2 A_1 sin.)	Ti-e_g d_{z^2} (A_1)	E	
	O p_z (B_1)	Ti-e_g $d_{x^2-y^2}$ (B_1)	E	
	O p_x, p_y (3 E dup.)	Ti-t_{2g} d_{xz}, d_{yz} (E)	A_1, A_2, B_1, B_2	◇
χ_{xxz}	O p_z (2 A_1 sin.)	Ti-t_{2g} d_{xz}, d_{yz} (E)	A_1, E	◇
	O p_z (B_1)	Ti-t_{2g} d_{xz}, d_{yz} (E)	B_1, E	
	O p_x, p_y (3 E dup.)	Ti-t_{2g} d_{xy} (B_2)	B_2, E	◇
	O p_x, p_y (3 E dup.)	Ti-e_g d_{z^2} (A_1)	A_1, E	
	O p_x, p_y (3 E dup.)	Ti-e_g $d_{x^2-y^2}$ (B_1)	B_1, E	

[a]The diamond symbol (◇) denotes the optical transitions which are expected to have the lowest energy.

more complex as it includes all $\hat{\chi}$ elements). This has been demonstrated by a very recent experiment on LAO/STO interfaces [27].

Briefly, in this work SHG spectra in the SHG photon-energy range between 3.2 and 4.2 eV have been measured at the three aforementioned polarization combinations (below 3.2 eV, all SHG spectra are featureless). The *pp* SHG spectrum displays a peak at about 3.8–4.0 eV, that has been ascribed to the known valence-to-conduction band edge [37]. At 3.6 eV, an additional peak is present that was previously attributed to a surface subband [25]. Interestingly this peak is completely absent in the *sp* spectrum, a clear evidence of the action of a symmetry selection rule. In particular, the 3.6 eV peak must be assigned to a transition that is symmetry-allowed in χ_{xxz} and forbidden in χ_{zxx}. According to our results, possible candidates are: (i) O $p_x, p_y \rightarrow$ Ti-t_{2g} d_{xy}, and (ii) O $p_z(A_1) \rightarrow$ Ti-t_{2g} d_{xz}, d_{yz}. Angle-resolved photoemission spectroscopy data on $SrTiO_3$ surfaces 38]] and x-ray absorption spectroscopy [19] on LAO/STO show that the lowest conduction band is given by d_{xy} orbitals, but this is not enough to assign unambiguously a definite energy sequence to these two transitions, because the optical transition energies are obviously also affected by the valence band. However, it is likely that both these two transitions affect the low-energy part of the SHG spectrum.

Once given these attributions for the 3.6 eV peak, the highest part of the SHG spectra, that is beyond 3.6 eV, is presumably dominated by the O p_x, $p_y \rightarrow$ Ti-t_{2g} d_{xz}, d_{yz} transitions. The O $p_z B_1 \rightarrow$ Ti-t_{2g} d_{xz}, d_{yz} E transition can be safely excluded, instead, because O $p_z B_1$ (corresponding to Γ_{25} in the bulk STO) is expected to be lower in energy by at least 1 eV with respect to O $p_z A_1$ at the Γ point (2 eV in the data from [38]). Therefore, the *sp*-polarized signal of SHG is expected to exhibit a much larger spectral weight above 3.6 eV, as compared with the *ds*-polarized one. This can be deduced from Table 2, where the O p_x, $p_y \rightarrow$ Ti-t_{2g} d_{xz}, d_{yz} transition is seen to be allowed only for the χ_{zxx} tensor component, while it is forbidden for the other two components. Also this prediction has been confirmed by the experiment reported in [27].

6. CONCLUSION

In conclusion, we have reported a theoretical analysis of the symmetries and spectral transitions that are relevant for the second-order nonlinear optical response of oxide interfaces with cubic symmetry. In particular, we discuss the case of $LaAlO_3/SrTiO_3$ interfaces. We show that the symmetry analysis leads to selection rules that affect the spectra recorded with different polarization combinations of light. Based on this analysis, we put forward a possible explanation of recent experimental observations in spectroscopic SHG. In particular, we provide a theoretical justification for the assignment of the lowest energy part of the SHG spectra to the O $p_x, p_y \rightarrow$ Ti-t_{2g} d_{xy} and/or O p_z $(A_1) \rightarrow$ Ti-t_{2g} d_{xz}, d_{yz} transitions.

We stress here that much of our analysis is not limited to the case of LAO/STO interfaces, but it may be readily applied to a wider range of polar/nonpolar interfaces that share the same symmetry properties. In particular it would be interesting to measure the spectra of other promising STO-based interfaces (for example $NdGaO_3/SrTiO_3$ and $LaGaO_3/SrTiO_3$ [39]) or when varying external parameters, as temperature. In both cases the symmetry properties of the interface are not altered and hence the qualitative behavior of the spectra, as discussed above, should be the same.

If this prediction will be confirmed by experiments, we can eventually reckon on universal selection rules that in turn might contribute to a better understanding of the physics of these interfaces.

ACKNOWLEDGMENTS

We acknowledge funding from the European Union (Programme FP7/2007-2013, grant agreement nos. 264098-MAMA and 228989-OxIDes), and by the Ministero dell'Istruzione, dell'Università e della Ricerca (grant PRIN 2010-11—OXIDE).

REFERENCES

1. R. Ramesh and D. G. Schlom, "Whither oxide electronics?" MRS Bull. **33**, 1006–1014 (2008).
2. A. Ohtomo and H. Hwang, "A high-mobility electron gas at the $LaAlO_3/SrTiO_3$ heterointerface," Nature **427**, 423–426 (2004).
3. N. Nakagawa, H. Y. Hwang, and D. A. Muller, "Why some interfaces cannot be sharp," Nat. Mater. **5**, 204–209 (2006).
4. S. Thiel, G. Hammerl, A. Schmehl, C. Schneider, and J. Mannhart, "Tunable quasi-two-dimensional electron gases in oxide heterostructures," Science **313**, 1942–1945 (2006).
5. A. Brinkman, M. Huijben, M. V. Zalk, J. Huijben, U. Zeitler, J. C. Maan, W. G. V. der Wiel, G. Rijnders, D. H. A. Blank, and H. Hilgenkamp, "Magnetic effects at the interface between non-magnetic oxides," Nat. Mater. **6**, 493–496 (2007).
6. N. Reyren, S. Thiel, A. Caviglia, L. Fitting Kourkoutis, G. Hammerl, C. Richter, C. Schneider, T. Kopp, A.-S. Rüetschi, D. Jaccard, M. Gabay, D. Muller, J.-M. Triscone, and J. Mannhart, "Superconducting interfaces between insulating oxides," Science **317**, 1196–1199 (2007).
7. C. Cen, S. Thiel, G. Hammerl, C. Schneider, K. Andersen, C. Hellberg, J. Mannhart, and J. Levy, "Nanoscale control of an interfacial metal-insulator transition at room temperature," Nat. Mater. **7**, 298–302 (2008).
8. M. Basletic, J.-L. Maurice, C. Carrétéro, G. Herranz, O. Copie, M. Bibes, E. Jacquet, K. Bouzehouane, S. Fusil, and A. Barthélémy, "Mapping the spatial distribution of charge carriers in $LaAlO_3/SrTiO_3$ heterostructures," Nat. Mater. **7**, 621–625 (2008).
9. K. Yoshimatsu, R. Yasuhara, H. Kumigashira, and M. Oshima, "Origin of metallic states at the heterointerface between the band insulators $LaAlO_3$ and $SrTiO_3$," Phys. Rev. Lett. **101**, 026802 (2008).
10. A. Caviglia, S. Gariglio, N. Reyren, D. Jaccard, T. Schneider, M. Gabay, S. Thiel, G. Hammerl, J. Mannhart, and J.-M. Triscone, "Electric field control of the $LaAlO_3/SrTiO_3$ interface ground state," Nature **456**, 624–627 (2008).
11. M. Huijben, A. Brinkman, G. Koster, G. Rijnders, H. Hilgenkamp, and D. H. A. Blank, "Structure-property relation of $SrTiO_3/LaAlO_3$ interfaces," Adv. Mater. **21**, 1665–1677 (2009).
12. P. Zubko, S. Gariglio, M. Gabay, P. Ghosez, and J.-M. Triscone, "Interface physics in complex oxide heterostructures," Annu. Rev. Condens. Matter Phys. **2**, 141–165 (2011).
13. M. Huijben, G. Rijnders, D. H. A. Blank, S. Bals, S. V. Aert, J. Verbeeck, G. V. Tendeloo, A. Brinkman, and H. Hilgenkamp, "Electronically coupled complementary interfaces between perovskite band insulators," Nat. Mater. **5**, 556–560 (2006).
14. A. Tsukazaki, A. Ohtomo, T. Kita, Y. Ohno, H. Ohno, and M. Kawasaki, "Quantum Hall effect in polar oxide heterostructures," Science **315**, 1388–1391 (2007).
15. Y. Hotta, T. Susaki, and H. Y. Hwang, "Polar discontinuity doping of the $LaVO_3/SrTiO_3$ interface," Phys. Rev. Lett. **99**, 236805 (2007).
16. T. Higuchi, Y. Hotta, T. Susaki, A. Fujimori, and H. Y. Hwang, "Modulation doping of a Mott quantum well by a proximate polar discontinuity," Phys. Rev. B **79**, 075415 (2009).
17. H. Hwang, "Tuning interface states," Science **313**, 1895–1896 (2006).
18. C. Cen, S. Thiel, J. Mannhart, and J. Levy, "Oxide nanoelectronics on demand," Science **323**, 1026–1030 (2009).

19. M. Salluzzo, J. Cezar, N. Brookes, V. Bisogni, G. De Luca, C. Richter, S. Thiel, J. Mannhart, M. Huijben, A. Brinkman, G. Rijnders, and G. Ghiringhelli, "Orbital reconstruction and the two-dimensional electron gas at the $LaAlO_3/SrTiO_3$ interface," Phys. Rev. Lett. **102**, 166804 (2009).
20. M. Sing, G. Berner, K. Groß, A. Müller, A. Ruff, A. Wetscherek, S. Thiel, J. Mannhart, A. Pauli, C. Schneider, P. Willmott, M. Gorgoi, F. Schäfers, and R. Claessen, "Profiling the interface electron gas of $LaAlO_3/SrTiO_3$ heterostructures with hard x-ray photoelectron spectroscopy," Phys. Rev. Lett. **102**, 176805 (2009).
21. S. Seo, M. Han, G. Hassink, W. Choi, S. Moon, J. Kim, T. Susaki, Y. Lee, J. Yu, C. Bernhard, H. Hwang, G. Rijnders, D. Blank, B. Keimer, and T. Noh, "Two-dimensional confinement of $3d^1$ electrons in $LaTiO_3/LaAlO_3$ multilayers," Phys. Rev. Lett. **104**, 036401 (2010).
22. L. Marrucci, D. Paparo, G. Cerrone, C. de Lisio, E. Santamato, S. Solimeno, S. Ardizzone, and P. Quagliotto, "Probing interfacial properties by optical second-harmonic generation," Opt. Lasers Eng. **37**, 601–610 (2002).
23. A. Savoia, D. Paparo, P. Perna, Z. Ristic, M. Salluzzo, F. Miletto Granozio, U. Scotti di Uccio, C. Richter, S. Thiel, J. Mannhart, and L. Marrucci, "Polar catastrophe and electronic reconstructions at the $LaAlO_3/SrTiO_3$ interface: evidence from optical second harmonic generation," Phys. Rev. B **80**, 075110 (2009).
24. N. Ogawa, K. Miyano, M. Hosoda, T. Higuchi, C. Bell, Y. Hikita, and H. Hwang, "Enhanced lattice polarization in $SrTiO_3/LaAlO_3$ superlattices measured using optical second-harmonic generation," Phys. Rev. B **80**, 081106 (2009).
25. A. Rubano, M. Fiebig, D. Paparo, A. Marino, D. Maccariello, U. Scotti di Uccio, F. Miletto Granozio, L. Marrucci, C. Richter, S. Paetel, and J. Mannhart, "Spectral and spatial distribution of polarization at the $LaAlO_3/SrTiO_3$ interface," Phys. Rev. B **83**, 155405 (2011).
26. T. Güenter, A. Rubano, D. Paparo, M. Lilienblum, L. Marrucci, F. Miletto Granozio, U. Scotti di Uccio, R. Jany, C. Richter, J. Mannhart, and M. Fiebig, "Spatial inhomogeneities at the $LaAlO_3/SrTiO_3$ interface: evidence from second harmonic generation," Phys. Rev. B **86**, 235418 (2012).
27. A. Rubano, T. Güenter, T. Fink, D. Paparo, L. Marrucci, C. Cancellieri, S. Gariglio, J.-M. Triscone, and M. Fiebig, "Influence of atomic termination on the $LaAlO_3/SrTiO_3$ interfacial polar rearrangement," Phys. Rev. B **88**, 035405 (2013).
28. J. F. Ward, "Calculation of nonlinear optical susceptibilities using diagrammatic perturbation theory," Rev. Mod. Phys. **37**, 1–18 (1965).
29. E. Luppi, H. Hübener, and V. Véniard, "*Ab initio* second-order nonlinear optics in solids: second-harmonic generation spectroscopy from time-dependent density-functional theory," Phys. Rev. B **82**, 235201 (2010).
30. M. Bertocchi, E. Luppi, E. Degoli, V. Véniard, and S. Ossicini, "Large crystal local-field effects in second-harmonic generation of a Si/CaF2 interface: an *ab initio* study," Phys. Rev. B **86**, 035309 (2012).
31. R. W. Boyd, *Nonlinear Optics* (Academic, 2003).
32. D. C. Hutchings and J. M. Arnold, "Determination of second-order nonlinear coefficients in semiconductors using pseudo-spin equations for three-level systems," Phys. Rev. B **56**, 4056–4067 (1997).
33. D. C. Harris and M. D. Bertolucci, *Symmetry and Spectroscopy: An Introduction to Vibrational and Electronic Spectroscopy* (Dover, 1989).
34. A. H. Kahn and A. J. Leyendecker, "Electronic energy bands in strontium titanate," Phys. Rev. **135**, A1321–A1325 (1964).
35. L. F. Mattheiss, "Energy bands for $KNiF_3$, $SrTiO_3$, $KMoO_3$, and $KTaO_3$," Phys. Rev. B **6**, 4718–4740 (1972).
36. K. van Benthem, C. Elsässer, and R. H. French, "Bulk electronic structure of $SrTiO_3$: experiment and theory," J. Appl. Phys. **90**, 6156–6164 (2001).
37. W. Luo, W. Duan, S. G. Louie, and M. L. Cohen, "Structural and electronic properties of n-doped and p-doped $SrTiO_3$," Phys. Rev. B **70**, 214109 (2004).
38. A. F. Santander-Syro, O. Copie, T. Kondo, F. Fortuna, S. Pailhes, R. Weht, X. G. Qiu, F. Bertran, A. Nicolaou, A. Taleb-Ibrahimi, P. Le Fevre, G. Herranz, M. Bibes, N. Reyren, Y. Apertet, P. Lecoeur, A. Barthelemy, and M. J. Rozenberg, "Two-dimensional electron gas with universal subbands at the surface of $SrTiO_3$," Nature **469**, 189–193 (2011).
39. C. Cantoni, J. Gazquez, F. M. Granozio, M. P. Oxley, M. Varela, A. R. Lupini, S. J. Pennycook, C. Aruta, U. Scotti di Uccio, P. Perna, and D. Maccariello, "Electronic transfer and ionic displacements as the origin of the 2D electron gas at the LAO/STO interface: direct measurements with atomic-column spatial resolution," Adv. Mater. **24**, 3952–3957 (2012).